Inelastic Transversely Isotropic Constitutive Model for High Performance Polymer Fibers

Subramani Sockalingam[1,2], John W. Gillespie Jr. [1,2,3,4], Michael Keefe[1,2]

[1]*Center for Composite Materials, University of Delaware, DE, USA*
[2]*Department of Mechanical Engineering, University of Delaware, DE, USA*
[3]*Department of Materials Science and Engineering, University of Delaware, DE, USA*
[4]*Department of Civil and Environmental Engineering, University of Delaware, DE, USA*

Abstract

High performance polymer fibers such as Kevlar, Spectra and Dyneema are widely used in ballistic impact applications. Under transverse compression at finite strains these fibers exhibit nonlinear inelastic behavior. The role of transverse compression during ballistic impact is not very well understood. In this work we implement a transversely isotropic inelastic constitutive model as a user defined material model (UMAT) in LS-DYNA®. A plasticity approach is used to model the material nonlinearity and a pseudo-elastic approach for the large residual strains in the transverse fiber plane. Based on the experimental results, the material nonlinearity and inelasticity are decoupled from the fiber direction. The UMAT predictions for a single Kevlar KM2 fiber under transverse compression are compared to the experimental load deflection under monotonic and cyclic loading.

Introduction

High performance polymer fibers lend itself to high velocity impact (HVI) energy absorbing applications due to their superior specific strength and specific modulus. Kevlar KM2 is one such fiber that is widely used in ballistic applications [1,2] in the form of flexible textile fabrics. These textile fabrics possess a hierarchical multi-scale architecture with different length scales from fibers to yarns (bundle of fibers) to woven fabrics. These fibers, in general, exhibit transverse isotropy with linear elastic behavior in longitudinal tension and nonlinear inelastic behavior in transverse (diametral) compression [3,4]. The micro-fibrillar structure of Kevlar aramid fibers based on poly (para-phenylene terephathalaide) (PPTA) has been studied by various researchers [5,6]. The fiber length scale is comprised of a collection of oriented micro-fibrils with van der Waals type non-bonded interactions [7]. An atomic force microscopy (AFM) phase image of a Kevlar KM2 fiber obtained by McAllister et al. [8] is reproduced below in Figure 1. They measured fibril diameters in the range of 10-50 nm.
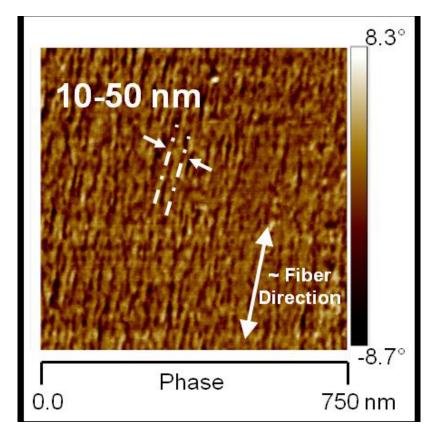
Figure 1. AFM image of Kevlar KM2 [9] (reproduced with permission)

Significant transverse compressive stresses are imposed on the fibers underneath the impactor. The experimental results reported in the literature are at the yarn length scale [10] and fabric length scale [11]. The role of the transverse properties of these fibers and fundamental fiber-level mechanisms during a HVI event are not very well understood. The transverse compression contribution is, in general, neglected by the homogenized numerical modeling approaches commonly used in the literature [3,12-16]. The fiber length scale modeling digital element method (DEM) reported in the literature [17,18] used a few 1D rod elements (19-fibers) to represent hundreds of fibers in a yarn. They account for the transverse properties of the fibers by specifying them as contact stiffness in the contact algorithm for fiber-fiber contact. However DEM does not account for the effect of Poisson's ratio and the subsequent growth in large contact width that is experimentally observed [19]. The longitudinal shear deformation mode also cannot be modeled by the DEM which may play a role in the failure of fibers [20].

The authors of this paper systematically investigated the transverse compression response of a Kevlar KM2 single fiber and tow using a 'bottom-up' approach by explicitly modeling all the 400 fibers in a tow [21,22]. However the constitutive model used in the previous study does not account for the material nonlinearity and large residual strains associated with the inelastic behavior. In this work we implement a simple nonlinear inelastic model to capture the experimentally observed residual strains in cyclic loading of the fiber under large transverse compressive strains.

Single Fiber Transverse Compression

The schematic of single fiber transverse compression and the experimental nominal stress-nominal strain response reported by Cheng et al. [4] for a Kevlar KM2 fiber of 12 μm diameter is shown in Figure 2. Nominal stress is defined as load per unit length divided by the original fiber diameter and nominal strain is defined as the platen displacement divided by the original fiber diameter. The experimental response is nonlinear and inelastic under large compressive strains with both material and geometric nonlinearities. They measured large residual transverse deformation at a very small nominal strain level of 0.075. In addition they compared the cyclic response of the fiber in compression to the Mullin's effect in rubber. The primary loading path is *OA* and upon first unloading path *AB* is followed. Reloading follows path *BA* with some deviation (not shown) and further loading turns into primary loading of the virgin material. Singletary et al. [23] hypothesized yielding followed by fibrillation for Kevlar 29 fibers. Phoenix and Skelton [24] also noted some fibrillation and computed a shear yield stress of 46 MPa for Kevalr 29 fibers.
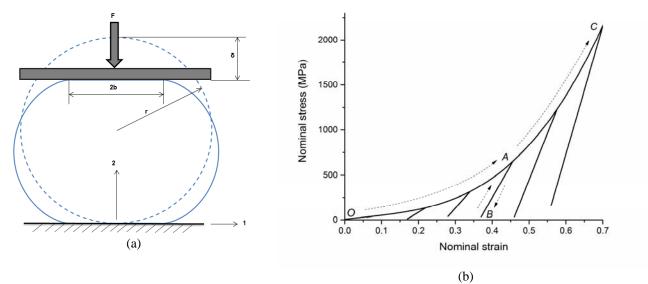

(a)

(b)

Figure 2. (a) Schematic of single fiber transverse compression (b) Smoothed experimental nominal stress-nominal strain [4] (compressive stress and strain shown positive)

Analytical linear elastic solutions proposed for the Hertzian contact problem is in general utilized to estimate the transverse modulus of the fiber. Cheng et al. [4] estimated an elastic transverse modulus of 1.34 ± 0.35 GPa by fitting the small strain experimental results to the analytical solution assuming an in plane Poisson's ratio of 0.24. Our earlier study [22] indicated even at very small strains the assumption of the Hertzian contact problem, namely, contact half width much smaller than the radius of the fiber $b << r$ does not hold. Therefore we numerically studied the single fiber transverse compression using finite element (FE) simulations with a 2D plane strain model using properties shown in Table 1. A minimum number of 84 elements were required to discretize the fiber cross section to accurately capture the fiber response under large compressive strains.

Table 1. Transversely isotropic properties of Kevlar KM2 single fiber [4]

ρ (g/cm³)	d (μm)	E₁ (GPa)	E₃ (GPa)	G₁₃ (GPa)	ν₃₁	ν₁₂
1.44	12.0	1.34	84.62	24.40	0.60	0.24

The constitutive model used in our previous study (*MAT_022) does not consider the material nonlinearity and inelastic strains. The experimental results indicate large inelastic strains in the transverse plane (12-plane), a linear elastic behavior in the fiber direction (3-direction) in tension until failure and possible degradation of tensile strength after transverse compression [4,25]. Various orthotropic constitutive models for composite materials are available in LS-DYNA. For example, *MAT_022 and *MAT_054-055 offers linear elastic behavior with different failure modes, *MAT_162 a continuum damage mechanics based model for softening and progressive damage. However none of the available models offer all the required features to model the behavior of fibers. Therefore we implement a UMAT suitable for LS-DYNA explicit analysis.

Constitutive Model Implementation in UMAT

The constitutive model is implemented within the framework of orthotropic incremental formulation for solid elements. The stress strain relation for an orthotropic material is given by:

$$
\begin{bmatrix} \sigma_1 \\ \sigma_2 \\ \sigma_3 \\ \sigma_4 \\ \sigma_5 \\ \sigma_6 \end{bmatrix} = \begin{bmatrix} C_{11} & C_{12} & C_{13} & 0 & 0 & 0 \\ C_{12} & C_{22} & C_{23} & 0 & 0 & 0 \\ C_{13} & C_{23} & C_{33} & 0 & 0 & 0 \\ 0 & 0 & 0 & C_{44} & 0 & 0 \\ 0 & 0 & 0 & 0 & C_{55} & 0 \\ 0 & 0 & 0 & 0 & 0 & C_{66} \end{bmatrix} \begin{bmatrix} \varepsilon_1 \\ \varepsilon_2 \\ \varepsilon_3 \\ \gamma_4 \\ \gamma_5 \\ \gamma_6 \end{bmatrix}
\tag{1}
$$

where the stiffness coefficients are given by:

$$
\begin{aligned}
&C_{11} = \frac{(1 - \nu_{23}\nu_{32})E_1}{S} \quad C_{44} = G_{12} \\[2mm]
&C_{22} = \frac{(1 - \nu_{13}\nu_{31})E_2}{S} \quad C_{55} = G_{23} \\[2mm]
&C_{33} = \frac{(1 - \nu_{12}\nu_{21})E_3}{S} \quad C_{66} = G_{31} \\[2mm]
&C_{12} = \frac{(\nu_{21} + \nu_{31}\nu_{23})E_1}{S} \quad \frac{\nu_{ij}}{E_i} = \frac{\nu_{ji}}{E_j} \ (\text{for } i, j = 1, 2, 3) \\[2mm]
&C_{23} = \frac{(\nu_{32} + \nu_{31}\nu_{12})E_2}{S} \\[2mm]
&C_{13} = \frac{(\nu_{31} + \nu_{21}\nu_{32})E_1}{S} \\[2mm]
&S = 1 - \nu_{12}\nu_{21} - \nu_{23}\nu_{32} - \nu_{13}\nu_{31} - 2\nu_{21}\nu_{32}\nu_{13}
\end{aligned}
\tag{2}
$$

Several possibilities exist to model the material nonlinearity and permanent deformation of the fiber in the 12-plane. Here we adopt a plasticity approach in the 12-plane for the material nonlinearity. A plane stress von Mises isotropic linear hardening plasticity algorithm is implemented in the UMAT such that material nonlinearity and residual strains are decoupled from the fiber direction. The plasticity algorithm is similar to *MAT_003 and is briefly outlined below. The detailed plasticity theory is given in [26].

1. Elastic trial stress update

$$\sigma_{ij}^{trial} = \sigma_{ij}^{n} + C_{ijkl}\Delta\varepsilon_{kl} \quad \text{(for } i, j = 1, 2) \tag{3}$$

2. Check yield condition

$$\phi^{trial} = 3J_2^{trial} - \sigma_y^2 \text{ (for } i, j = 1, 2)$$

$$\text{where } J_2^{trial} = \frac{1}{2}s_{ij}^{trial}s_{ij}^{trial}, s_{ij}^{trial} = \sigma_{ij}^{trial} - \frac{1}{3}\sigma_{kk}^{trial} \text{ and } \sigma_y^{n+1} = \sigma_o + E_p\varepsilon^{p^n} \tag{4}$$

$$E_p = \frac{E_1 E_t}{E_1 - E_t} \text{ where } E_t \text{ is the tangent modulus}$$

σ_o, E_p and ε^p are initial yield stress, plastic hardening modulus and effective plastic strain respectively.

IF $\phi^{trial} = 3J_2^{trial} - \sigma_y^2 \leq 0$ then the trial stresses are within the yield surface and accept the trial stresses as the solution for the current time step $\sigma_{ij}^{n+1} = \sigma_{ij}^{trial}$ and EXIT.

3. ELSE incremental plastic strain is computed using the consistency condition and associative flow rule. A single-equation return mapping is used to scale the deviatoric stresses as given below.

$$\Delta\lambda = \frac{\phi^{trial}}{3G_{12} + E_p} \quad \varepsilon^{p^{n+1}} = \varepsilon^{p^n} + \Delta\lambda$$

$$\sigma_{ij}^{n+1} = \sigma_{ij}^{trial} - \frac{\Delta\lambda 3G_{12}}{\sqrt{3J_2^{trial}}}s_{ij}^{trial} \quad \text{(for } i, j = 1, 2) \tag{5}$$

For plane stress plasticity in the 12-plane the correct plastic strain increment is computed by enforcing pseudo stress $\sigma_{33}^{pseudo} = 0$. Secant iterations are performed with two starting values for the pseudo normal strain increment $\Delta\varepsilon_{33}^{pseudo,1} = -\dfrac{C_{13}\Delta\varepsilon_{11} + C_{23}\Delta\varepsilon_{22}}{C_{33}}$ and

$\Delta\varepsilon_{33}^{pseudo,2} = -(\Delta\varepsilon_{11} + \Delta\varepsilon_{22})$. The plasticity algorithm is called for both starting values to compute the corresponding pseudo normal stresses. The pseudo normal strain increment is then computed as

$$\Delta\varepsilon_{33}^{pseudo,i+1} = \Delta\varepsilon_{33}^{pseudo,i} - \frac{\Delta\varepsilon_{33}^{pseudo,i} - \Delta\varepsilon_{33}^{pseudo,i-1}}{\Delta\sigma_{33}^{pseudo,i} - \Delta\sigma_{33}^{pseudo,i-1}}\Delta\sigma_{33}^{pseudo,i}$$

Convergence condition for the iteration is given by $\dfrac{\left|\Delta\varepsilon_{33}^{pseudo,i+1} - \Delta\varepsilon_{33}^{pseudo,i}\right|}{\left|\Delta\varepsilon_{33}^{pseudo,i+1}\right|} < 10^{-4}$.

The stresses in the 3-direction are updated as

$$\sigma_{ij}^{n+1} = \sigma_{ij}^{n} + C_{ijkl}\Delta\varepsilon_{kl} \text{ (for } i = 1, 2 \text{ and } j = 3) \tag{6}$$

The plane stress plasticity implementation is verified by comparing the response of a single solid element (reduced integration) subjected to loading in 12-plane to a plane stress element using *MAT_003. The bottom four nodes of the unit cube shown in Figure 3(a) are constrained in the 2-direction and top four nodes are prescribed with a displacement boundary condition. Isotropic properties shown in Table 2 are used to make comparisons to the isotropic model *MAT_003.

Table 2. Isotropic properties used for verification

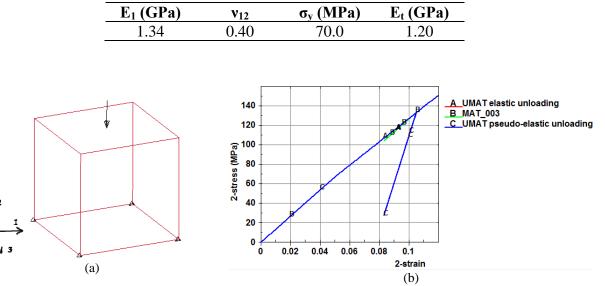| E$_1$ (GPa)	v$_{12}$	σ$_y$ (MPa)	E$_t$ (GPa)
1.34	0.40	70.0	1.20

(a)

(b)

Figure 3. (a) Unit cube with uniaxial cyclic loading (b) Stress strain response

It should be noted that compressive stresses and strains are shown positive throughout this paper. The stress strain and effective plastic strain predicted by UMAT in a cyclic load-unload-reload is identical to *MAT_003 as shown by curves A and B in Figure 3(b). However large inelastic strains are seen in the experimental response referring to Figure 2(b). To account for the large inelastic strains, a pseudo-elastic behavior is implemented during unloading and reloading. The idea of pseudo-elasticity is to describe the loading path as an elastic material (generally nonlinear) and the unloading path as another elastic material [27,28]. The load reversal is tracked within the UMAT and stress update for the normal stresses in the 12-plane is given by:

$$\sigma_{i}^{n+1} = \sigma_{i}^{n+1} + \frac{1}{c}\left(\varepsilon_{i} - \varepsilon_{i,\max}\right) \text{ (for } i = 1, 2) \tag{7}$$

where c is a parameter to control the slope of the unloading path and $\varepsilon_{i,max}$ is the maximum strain experienced by the material during the loading history. The additive term in Equation 7 is active only during unloading and reloading up to the point of load reversal. The UMAT has been implemented with options for either elastic unloading or pseudo-elastic unloading. The stress strain curve with pseudo-elastic unloading (for $1/c = 3.5$) is shown in Figure 3(b).

Next equal bi-axial strains in the 12-plane is applied to the unit cube element with the isotropic properties in Table 2. Identical stress strain and effective plastic strain is predicted for both UMAT and *MAT_003 as shown in Figure 4(b).

Figure 4. (a) Unit cube with biaxial cyclic loading (b) Stress strain response

Table 3. Transversely isotropic properties

E₁ (GPa)	ν₁₂ (GPa)	σᵧ (MPa)	Eₜ (GPa)	E₃ (GPa)	G₁₃ (GPa)	ν₃₁
1.34	0.40	70.0	1.20	84.62	24.40	0.60

The UMAT essentially combines *MAT_003 plane stress for the 12-plane and *MAT_022 (orthotropic linear elastic) for the 3-direction. The unit cube with uniaxial cyclic loading shown in Figure 3(a) is used with transversely isotropic properties in Table 3. The stress strain and effective plastic strain in the 12-plane for the UMAT agrees with the *MAT_003 plane stress element as shown in Figure 5. The stress in the 3-direction also agrees well with *MAT_022.
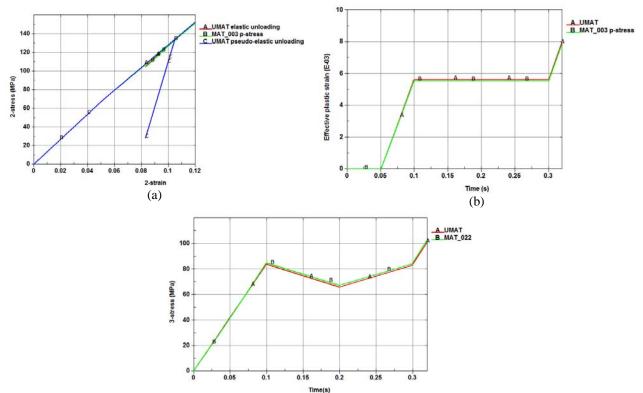
(a)

(b)

Figure 5. Uniaxial cyclic loading (a) Stress strain response in 12-plane (b) Effective plastic strain (c) 3-direction stress

Finite Element Model for Single Fiber Transverse Compression

The quarter symmetric FE model for single fiber transverse compression response shown in Figure 6 is constructed using reduced integration eight noded solid elements with unit thickness. The full fiber cross section is modeled with 84 elements which was determined through a mesh convergence study from our previous work [22]. Plane strain conditions are imposed by constraining the out of plane degree of freedom. The rigid platen is modeled using the *RIGIDWALL_GEOMETRIC_FLAT_MOTION. A coefficient of friction of 0.2 is used between the rigid wall and the fiber. The rigid platen is prescribed with a constant velocity to compress the fiber under monotonic loading. The nodes of the fiber are defined as slave nodes to the rigid wall. The penetrating slave nodes are moved back to the surface of the rigid wall [29]. The simulation is run with fiber properties shown in Table 4.
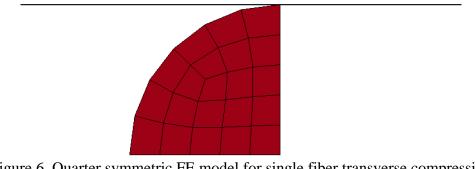

Figure 6. Quarter symmetric FE model for single fiber transverse compression

Table 4. Material properties for Kevlar KM2 single fiber

E_1 (GPa)	G_{12} (GPa)	σ_y (MPa)	E_t (GPa)	E_3 (GPa)	G_{13} (GPa)	v_{31}
1.34	0.40	70.0	1.20	84.62	24.40	0.60

The predicted nominal stress-nominal strain response using UMAT compares reasonably well to the experimental response as shown in Figure 7(a). The evolution of fiber cross section at different nominal strain levels is shown in Figure 7(b). It should be noted that contact half width approaches the change in diameter under very high strains as the circular fiber is deformed to a flat shape. At 70% nominal strain the diameter change is almost 100%.
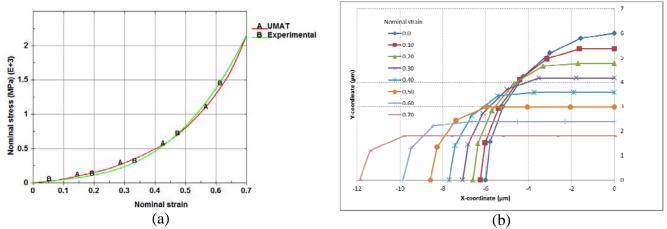

(a)   (b)

Figure 7. Monotonic loading (a) Nominal stress-nominal strain (b) Evolution of fiber cross section
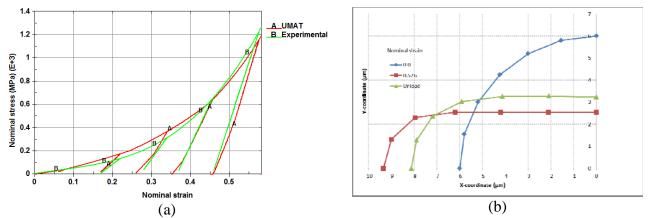

(a)   (b)

Figure 8. Cyclic loading (a) Nominal stress-nominal strain (b) Fiber cross section for load-unload

The UMAT is further used to simulate the cyclic loading of single fiber transverse compression. The predicted nominal stress-nominal strain response is shown in Figure 8. Relatively good correlation to the experimental response is provided by the UMAT with pseudo-elastic unloading. After each load-unload cycle large residual strains are accumulated. They may be attributed to the microstructural damage including damage of non-bonded interactions, fibrillation, and micro-cracking. This damage results in easier change in shape and the response looks like an almost incompressible behavior at higher strains. The fiber cross section for a nominal strain level of 0.576 (load level 14 N/mm) and the cross section after complete removal

of load are shown in Figure 8(b). After the removal of load irreversible growth in contact width and a diametral growth to about 16 µm is predicted by the simulation. This is consistent with our ongoing experimental efforts to measure the change in diameter for the fiber under large compressive strains to validate the UMAT. Figure 9 displays the laser and confocal microscopy image of a single Kevlar KM2 fiber of undeformed nominal diameter 12 µm compressed at load levels of 15 N/mm and 30 N/mm in an Instron Micro Tester.
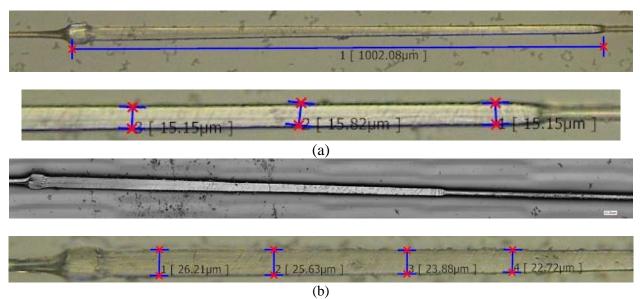

(a)

(b)

Figure 9. Deformed microscope image of a single Kevlar KM2 fiber (a) compressed at 15 N/mm (b) compressed at 30 N/mm

Conclusions

The experimental results for Kevlar fibers in transverse compression indicate nonlinear and inelastic behavior in the transverse plane and linear elastic behavior in tension in the fiber direction. This paper presented the implementation of a simple nonlinear inelastic constitutive model appropriate for high performance polymer fibers widely used in HVI applications. The model is implemented as a UMAT using incremental orthotropic formulation for explicit analysis with solid elements in LS-DYNA. The material nonlinearity is described using von Mises isotropic hardening plasticity. A pseudo-elastic approach is adopted to model the large residual strains in cyclic loading. The nonlinear and inelastic behavior is decoupled from the fiber direction. The implementation of the UMAT is verified using single element simulations. Single fiber transverse compression of Kevlar KM2 is simulated using the UMAT under monotonic and cyclic loading conditions. The nominal stress-nominal strain and diameter change predicted by the UMAT are found to compare reasonably well with the experimental results.

Acknowledgements

References

[1] Kim, J., McDonough, W.G., Blair, W., and Holmes, G.A., "The modified-single fiber test: A methodology for monitoring ballistic performance", *Journal of Applied Polymer Science,* Vol. 108, No. 2, 2008, pp. 876-886.
[2] Dong, Z., and Sun, C.T., "Testing and modeling of yarn pull-out in plain woven Kevlar fabrics", *Composites Part A: Applied Science and Manufacturing,* Vol. 40, No. 12, 2009, pp. 1863-1869.
[3] Grujicic, M., Bell, W.C., Arakere, G., He, T., Xie, X., and Cheeseman, B.A., "Development of a meso-scale material model for ballistic fabric and its use in flexible-armor protection systems", *Journal of Materials Engineering and Performance,* Vol. 19, No. 1, 2010, pp. 22-39.
[4] Cheng, M., Chen, W., and Weerasooriya, T., "Experimental investigation of the transverse mechanical properties of a single Kevlar® KM2 fiber", *International Journal of Solids and Structures,* Vol. 41, No. 22–23, 2004, pp. 6215-6232.
[5] Rao, Y., Waddon, A.J., and Farris, R.J., "The evolution of structure and properties in poly(p-phenylene terephthalamide) fibers", *Polymer,* Vol. 42, No. 13, 2001, pp. 5925-5935.
[6] McAllister, Q.P., Gillespie, J.W., and VanLandingham, M.R., "Evaluation of the three-dimensional properties of Kevlar across length scales", *Journal of Materials Research,* Vol. 27, No. 14, 2012, pp. 1824-1837.
[7] Grujicic, M., Glomski, P., Pandurangan, B., Bell, W., Yen, C., and Cheeseman, B., "Multi-length scale computational derivation of Kevlar® yarn-level material model", *Journal of Materials Science,* Vol. 46, No. 14, 2011, pp. 4787-4802.
[8] McAllister, Q.P., Gillespie Jr, J.W., and VanLandingham, M.R., "The influence of surface microstructure on the scratch characteriztics of Kevlar fibers", Vol. 48, No. 3, 2013, pp. 292-1302.
[9] McAllister, Q.P. , *The energy dissipative mechanisms of the particle-fiber interface in a textile composite,* 2013.
[10] Song, B., Park, H., Lu, W.-., and Chen, W., "Transverse impact response of a linear elastic ballistic fiber yarn", *Journal of Applied Mechanics,* Vol. 78, No. 5, 2011, .
[11] Tan, V.B.C., Lim, C.T., and Cheong, C.H., "Perforation of high-strength fabric by projectiles of different geometry", *International Journal of Impact Engineering,* Vol. 28, No. 2, 2003, pp. 207-222.
[12] Stahlecker, Z., Mobasher, B., Rajan, S.D., and Pereira, J.M., "Development of reliable modeling methodologies for engine fan blade out containment analysis. Part II: Finite element analysis", *International Journal of Impact Engineering,* Vol. 36, No. 3, 2009, pp. 447-459.
[13] Duan, Y., Keefe, M., Bogetti, T.A., and Cheeseman, B.A., "Modeling friction effects on the ballistic impact behavior of a single-ply high-strength fabric", *International Journal of Impact Engineering,* Vol. 31, No. 8, 2005, pp. 996-1012.
[14] Rao, M.P., Duan, Y., Keefe, M., Powers, B.M., and Bogetti, T.A., "Modeling the effects of yarn material properties and friction on the ballistic impact of a plain-weave fabric", *Composite Structures,* Vol. 89, No. 4, 2009, pp. 556-566.
[15] Rao, M.P., Nilakantan, G., Keefe, M., Powers, B.M., and Bogetti, T.A., "Global/Local Modeling of Ballistic Impact onto Woven Fabrics", *Journal of Composite Materials,* Vol. 43, No. 5, 2009, pp. 445-467.
[16] Nilakantan, G., Keefe, M., Bogetti, T.A., Adkinson, R., and Gillespie Jr., J.W., "On the finite element analysis of woven fabric impact using multiscale modeling techniques", *International Journal of Solids and Structures,* Vol. 47, No. 17, 2010, pp. 2300-2315.
[17] Wang, Y., Miao, Y., Swenson, D., Cheeseman, B.A., Yen, C., and LaMattina, B., "Digital element approach for simulating impact and penetration of textiles", *International Journal of Impact Engineering,* Vol. 37, No. 5, 2010, pp. 552-560.

[18] Grujicic, M., Hariharan, A., Pandurangan, B., Yen, C.-., Cheeseman, B.A., Wang, Y., Miao, Y., and Zheng, J.Q., "Fiber-level modeling of dynamic strength of Kevlar KM2 ballistic fabric", *Journal of Materials Engineering and Performance,* Vol. 21, No. 7, 2012, pp. 1107-1119.

[19] Lim, J., Zheng, J.Q., Masters, K., and Chen, W.W., "Effects of gage length, loading rates, and damage on the strength of PPTA fibers", *International Journal of Impact Engineering,* Vol. 38, No. 4, 2011, pp. 219-227.

[20] Ha-Minh, C., Imad, A., Boussu, F., Kanit, T., and Crépin, D., "Numerical study on the effects of yarn mechanical transverse properties on the ballistic impact behavior of textile fabric", *The Journal of Strain Analysis for Engineering Design,* 2012, .

[21] S. Sockalingam, J. W. Gillespie Jr. and M. Keefe. "Modeling the transverse compression response of Kevlar KM2", *American Society for Composites (ASC),* College Park, PA, 2013.

[22] Sockalingam, S., Gillespie Jr., J.W., and Keefe, M., "On the transverse compression response of Kevlar KM2 using fiber-level finite element model", *International Journal of Solids and Structures,* 2014, doi: http://dx.doi.org/10.1016/j.ijsolstr.2014.03.020, Article in Press.

[23] Singletary, J., Davis, H., Ramasubramanian, M.K., Knoff, W., and Toney, M., "The transverse compression of PPTA fibers Part I Single fiber transverse compression testing", *Journal of Materials Science,* Vol. 35, No. 3, 2000, pp. 573-581.

[24] Phoenix, S.L., and Skelton, J., "Transverse Compressive Moduli and Yield Behavior of Some Orthotropic, High-Modulus Filaments", *Textile Research Journal,* Vol. 44, No. 12, 1974, pp. 934-940.

[25] Cheng, M., Chen, W., and Weerasooriya, T., "Mechanical Properties of Kevlar® KM2 Single Fiber", *Journal of Engineering Materials and Technology,* Vol. 127, No. 2, 2005, pp. 197-203.

[26] de Souza Neto, Eduardo A, Peric, D., Owen, D.R.J. , *Computational methods for plasticity: theory and applications,* John Wiley & Sons, 2011.

[27] Ogden, R., and Roxburgh, D., "A pseudo–elastic model for the Mullins effect in filled rubber", *Proceedings of the Royal Society of London.Series A: Mathematical, Physical and Engineering Sciences,* Vol. 455, No. 1988, 1999, pp. 2861-2877.

[28] Holzapfel, G., Stadler, M., and Ogden, R., "Aspects of stress softening in filled rubbers incorporating residual strains", *Constitutive Models for Rubber,* 1999, pp. 189-193.

[29] Bala, S., "Choice of Rigidwall Treatment", URL: http://blog2.d3view.com/choice-of-rigidwall-treatment/. 03/18, 2014.